Edge-to-edge topological spectral transfer in diamond photonic lattices

Gabriel Cáceres-Aravena ; Bastián Real ; Diego Guzmán-Silva ; Paloma Vildoso ; Ignacio Salinas ;
Alberto Amo ; Tomoki Ozawa ; Rodrigo A. Vicencio ✉

Check for updates

CrossMark

View Online

Export Citation

Edge-to-edge topological spectral transfer in diamond photonic lattices

View Online   Export Citation   CrossMark

Gabriel Cáceres-Aravena,[1,2] [ID] Bastián Real,[1,2] [ID] Diego Guzmán-Silva,[1,2] [ID] Paloma Vildoso,[1,2] [ID] Ignacio Salinas,[1,2] [ID] Alberto Amo,[3] [ID] Tomoki Ozawa,[4] [ID] and Rodrigo A. Vicencio[1,2,a)] [ID]

AFFILIATIONS

[1] Departamento de Física, Facultad de Ciencias Físicas y Matemáticas, Universidad de Chile, Santiago, Chile
[2] Millennium Institute for Research in Optics–MIRO, Santiago, Chile
[3] Univ. Lille, CNRS, UMR 8523—PhLAM—Physique des Lasers Atomes et Molécules, F-59000 Lille, France
[4] Advanced Institute for Materials Research (WPI-AIMR), Tohoku University, Sendai 980-8577, Japan

[a)]Author to whom correspondence should be addressed: rvicencio@uchile.cl

ABSTRACT

The transfer of information between topological edge states is a robust way of spatially manipulating spatial states in lattice environments. This method is particularly efficient when the edge modes are kept within the topological gap of the lattice during the transfer. In this work, we show experimentally the transfer of photonic modes between topological edge states located at opposite ends of a dimerized one-dimensional photonic lattice. We use a diamond lattice of coupled waveguides and show that the topological transfer is insensitive to the presence of a high density of states in the form of a flat band at an energy close to that of the edge states and prevails in the presence of a hopping impurity. We explore the dynamics in the waveguide lattice using a wavelength-scan method, where different input wavelengths translate into different effective lattice lengths. Our results offer an alternative way to the implementation of efficient transfer protocols based on active driving mechanisms.
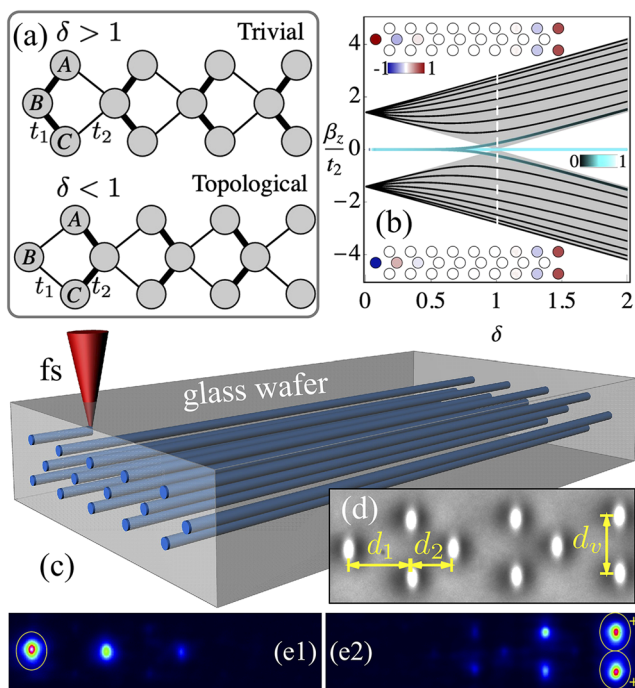
I. INTRODUCTION

Topological edge states are a remarkable resource for engineering photonic systems with isolated modes protected from the presence of disorder. In two-dimensional lattices, they can be used to fabricate topological edge mode lasers with distributed gain and quantized orbital momentum,[1,2] to transfer single photons around corners in elaborated photonic circuits,[3,4] and to design topological frequency combs with enhanced efficiency.[5,6] One-dimensional systems such as the Su-Schrieffer-Heeger (SSH) lattice are particularly interesting because topological edges and interface modes are hosted deep into the topological gap of the lattice. This gap protection has been shown to be beneficial in preserving the quantum state of photons in boundary modes.[7,8] Interestingly, the presence of topological edge modes on both sides of one-dimensional lattices can be used to transfer a state from one edge of the lattice to the other with high fidelity with the advantage of being protected from certain types of disorder due to the topological nature of the system. Such edge state transfer is a promising route to store and manipulate photonic quantum states in on-chip lattice environments.

Most topological edge transfer protocols rely on the adiabatic evolution of the lattice such that an edge mode is driven into quasi-bulk modes and again into an edge state at the other side.[9–17] While these protocols present an optimized transfer rate and fidelity, they are limited by the adiabaticity condition, which requires the adiabatic passage to be slow enough to avoid the Zenner coupling of the edge state information into the bulk modes.[18,19] Furthermore, the presence of disorder in the lattice would enhance this coupling. A variation of these protocols includes counter-adiabatic driving methods.[20] Recently, a rather different route has been proposed based on the coherent coupling of edge modes within the gap.[19,21,22] The great advantage of this approach is that edge modes are kept well into the topological gap throughout the protocol, ensuring high fidelity in reduced time. The simplest version of the coherent state transfer of topological edge states is via passive evanescent coupling of the exponential tails of edge modes at opposite sides of the finite size lattice. In this case, periodic oscillations between edge modes take place at a frequency determined by the tail overlap,[23] which can be controlled by the size of the gap. Observation of such coherent oscillations was reported in a short SSH lattice for Rydberg atoms.[24]

13 August 2023 13:13:42

In this work, we demonstrate coherent edge-to-edge transfer of light in dimerized diamond lattices of coupled optical waveguides by employing a spectral tomographic technique. First, we show that the orthogonality of eigenmodes in our undriven protocol preserves the transfer even in the presence of a high density of states in the form of a flat band (FB) at energies close to those of the edge states. Second, we demonstrate that the transfer mechanism persists in the presence of lattice defects thanks to the underlying chiral symmetry of the system. Our results offer a purely linear transfer of light via distant edge states, in strong contrast to, for example, the nonlinear switching in between two nearby topological interface states.[25] Additionally, the experimental proof of principle we report in this work can be significantly speeded up, for example, by applying a number of driven techniques based on the modulating of the hoppings in time and the use of concatenated topological lattices.[19,22,26]

II. THEORETICAL MODEL

To demonstrate the topological edge transfer, we use a diamond lattice[27–29] of coupled waveguides with different intracell (t_1) and intercell (t_2) hoppings, as sketched in Fig. 1(a). The lattice has

three sites per unit cell, denoted as A, B, and C sites. Considering a tight-binding coupled-mode approach, the evolution of the optical field at every site of the n-th unit cell is written as

$$-i\partial_z A_n = t_1 B_n + t_2 B_{n+1},$$
$$-i\partial_z B_n = t_1(A_n + C_n) + t_2(A_{n-1} + C_{n-1}), \qquad (1)$$
$$-i\partial_z C_n = t_1 B_n + t_2 B_{n+1}.$$

Here, A_n, B_n, and C_n are the amplitudes of the optical field at the n-th unit cell. z describes the coordinate along the waveguides and the dynamical variable. Moreover, the hopping strengths among nearest-neighbor (NN) sites can be varied experimentally by adjusting the lattice distances.[30] We then define the control parameter $\delta \equiv t_1/t_2$ to characterize the different regimes. We assume an infinite system and impose a Bloch-like *ansatz* in Eq. (1), obtaining the following bands:

$$\beta_z(k_x) = 0, \pm t_2\sqrt{2[\delta^2 + 2\delta\cos(k_x a) + 1]}, \qquad (2)$$

where β_z is the propagation constant (energy), a is the lattice constant, and k_x is the quasimomentum. The spectrum is composed of two dispersive and one flat band (FB) [see shaded areas and the horizontal light-blue line at $\beta_z = 0$ in Fig. 1(b), respectively]. The gap in between both dispersive bands has a size equal to $2\sqrt{2}t_2|\delta - 1|$. For $\delta = 1$, this gap closes, and the three bands touch each other at the edges of the Brillouin zone.[31] The diamond lattice possesses the smallest experimentally reported FB states,[31–33] with an inverse participation ratio (IPR)[34] of 1/2 [represented as a light-blue color in Fig. 1(b)]. Specifically, in the bases of Wannier functions in the A, B, and C sites, the FB eigenvector is given by: $|v^{FB}\rangle = \{1, 0, -1\}/\sqrt{2}$, and the ones corresponding to the dispersive bands are $|v^\pm\rangle = \{e^{i\phi(k_x)}, \pm\sqrt{2}, e^{i\phi(k_x)}\}/\sqrt{2}$, where $\phi(k_x) = \arctan(-\sin(k_x a)/[\delta + \cos(k_x a)])$.

Even though this lattice has three sites per unit cell, it exhibits similar topological features to the SSH model[35] when varying the parameter δ.[36] Indeed, a quantized Zak phase of value 0 or π can be found when $\delta > 1$ ($t_1 > t_2$) or $\delta < 1$ ($t_1 < t_2$), respectively. In this case, the nontrivial phase is protected by inversion symmetry between A_n and C_n, and by chiral symmetry.[36,37] Therefore, we expect the appearance of two edge states at a zero propagation constant on a lattice with open boundaries when $\delta < 1$. These two states are chiral partners and, therefore, one must have amplitude only at A sites, while the other must possess amplitude only at B and C sites. To corroborate this, we compute the spectrum as a function of δ for dimerized diamond lattices of 9 unit cells [see full lines in Fig. 1(b)]. It can be clearly seen that two states at zero frequency (lighter blue) transform into two dispersive states (darker blue) around $\delta = 1$. When increasing δ, the degeneracy between them is removed at around $\delta = 0.7$ [splitting $\Delta\beta_z^e \sim 0.06$, see Fig. S4(e) in the supplementary material] due to the finite size of the lattice. The flat band remains unchanged at $\beta_z = 0$, for any value of δ. The IPR (denoted by color) shows very clearly the transition from localized edge states (IPR = 1 or 1/2, light blue) into extended propagating modes (IPR $\sim 1/N$, black).

Figure 1(b) insets show the two edge states for $\delta = 0.4$. They exhibit exponentially localized amplitudes at both edges. On the left edge, these states present a null amplitude at A and C sites, whereas

FIG. 1. (a) Sketch of a dimerized diamond lattice, with A, B, and C as the sites of the unit cell. A thick (thin) line denotes strong (weak) hopping, and t_1 (t_2) indicates the intra(inter)-cell coupling constant. The top (bottom) panel schematizes the trivial (topological) case $t_1 > t_2$ ($t_1 < t_2$). (b) Spectrum as a function of δ for a finite (lines) and an infinite (shaded area) lattice. The vertical dashed line denotes $\delta = 1$. The color indicates the IPR for all the states. Inset: amplitude profiles of edge states at $\delta = 0.4$. (c) Sketch of the fs laser writing technique. (d) Microscope image of a diamond lattice with $\{d_1, d_2\} = \{35, 25\}$ μm ($\delta = 0.37$) and $d_v = 32$ μm. Output intensity profiles, after a propagation length of 7 cm, for (e1) a B left edge and (e2) an in-phase A–C right edge site excitations. Yellow ellipses indicate the excited sites.

the states have a null amplitude at B sites on the right edge. Moreover, one edge state is antisymmetric (bottom inset) and the other is symmetric (top inset) with respect to the opposite edge. They decay exponentially into the bulk as $(-\delta)^{|n-n_e|}$ for a semi-infinite system, exhibiting a phase shift of π at consecutive B or A, C sites, depending on the specific edge (n_e). For $\delta \gtrsim 0.7$, the frequency of the edge states deviates from 0 to $\pm\beta_z^e$. Therefore, the excitation of sites at the edges is expected to induce an oscillatory pattern in between both surfaces with a frequency β_z^e,[23] with a long-distance state transfer occurring on a large dynamical scale $z_{transfer} = \pi/\beta_z^e$ (see supplementary material.

Experimentally, the diamond lattice exhibits an important advantage compared to the SSH lattice because the bandgap is $\sqrt{2}$ wider for the diamond lattice, considering equal hopping strengths $t_{1,2}$; therefore, it reduces the possible coupling between edge and bulk modes in the presence of disorder in the couplings.

III. EXPERIMENTS AND ANALYSIS

We fabricate several dimerized diamond photonic lattices of 9 unit cells each by using a femtosecond (fs) laser writing technique,[30,38] as sketched in Fig. 1(c). For the first set of experiments, the diamond geometry is defined by distances d_1, d_2, and $d_v = 32$ μm, as described in Fig. 1(d). For these values, the diagonal (NN) distance was swept in the interval $\{25.6, 43.1\}$ μm, as d_1 and d_2 were varied in the interval $\{20, 40\}$ μm in steps of 1 μm. The hopping coefficients (which decay exponentially on waveguide separation[30]) range in the interval $\sim\{0.03, 0.21\}$ cm^{-1} at a wavelength of 640 nm. Figure 1(d) shows an output facet of a lattice with $d_1 = 35$ and $d_2 = 25$ μm, with $t_1 = 0.05$ and $t_2 = 0.14$ cm^{-1} ($\delta = 0.37$). We first test the quality of the lattices by exciting them at different input positions using a 640 nm laser beam (see supplementary material for a complete characterization). For example, topological edge states can be efficiently excited by injecting light directly at the lattice boundaries.[34,39,40] Figure 1(e1) shows the output profile after a B-edge site excitation, with a clear exponential decaying profile from the edge into the bulk. The excitation at the right boundary requires a more complicated input condition with two in-phase beams. The result of this is shown in Fig. 1(e2), with an output profile formed mostly by A and C sites.

We characterize the lattice dynamics by implementing a *wavelength-scan method*: The dynamics of a wavepacket injected into the input facet of a lattice are revealed when varying the input wavelength coming from a Supercontinuum (SC) laser source.[41-43] Therefore, instead of measuring the output profiles at different z values, which implies the fabrication of a larger number of lattices, we manipulate the input beam wavelength. The lattice dynamics depend on the excitation wavelength λ: the longer the wavelength, the wider the mode profile, and the larger the coupling constants[42] (see also the supplementary material). In this way, we can study the same lattice at different effective lengths by tuning the input wavelength.

We first consider a diamond lattice with $d_1 = d_2 = 30$ μm. We excite a B site at the central fifth unit cell and scan the input wavelength in the interval 600–760 nm, with a step of 10 nm. Figure 2(a) shows the output intensity for three selected λ's (a complete sweep is shown in supplementary material). Figure 2(b) shows the *second moment (width)*, defined as $m2 \equiv \sum_n (n - n_c)^2 P_n$, vs the input wavelength ($P_n \equiv |A_n|^2 + |B_n|^2 + |C_n|^2$, the unit cell power, and
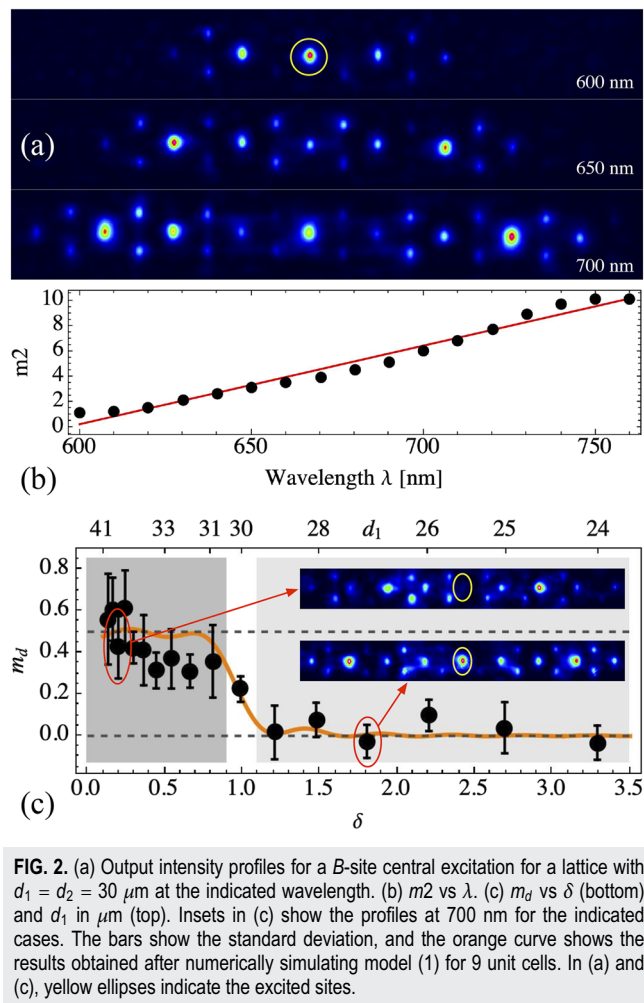
FIG. 2. (a) Output intensity profiles for a *B*-site central excitation for a lattice with $d_1 = d_2 = 30$ μm at the indicated wavelength. (b) $m2$ vs λ. (c) m_d vs δ (bottom) and d_1 in μm (top). Insets in (c) show the profiles at 700 nm for the indicated cases. The bars show the standard deviation, and the orange curve shows the results obtained after numerically simulating model (1) for 9 unit cells. In (a) and (c), yellow ellipses indicate the excited sites.

$n_c \equiv \sum_n n P_n$, the *center of mass*). We observe a growing diffraction pattern[33] with a width that increases almost linearly with the input wavelength [a linear fit is included in Fig. 2(b)]. $m2 \sim z$ corresponds to a ballistic regime,[44] as expected for discrete diffraction dynamics; therefore, a λ increment produces an effectively larger lattice propagation distance z or, equivalently, a larger coupling constant $t_{1,2}$.

A dimerized diamond lattice has two hoppings that simultaneously change while λ is modified. Since we observe a linear dependence of coupling constants on wavelength, we can assume δ as a constant as a first approximation. We use the wavelength-scan method to experimentally determine n_c for all the output profiles after exciting a B site at the central (fifth) unit cell of 17 dimerized lattices with different values of δ. For each lattice, we average n_c over λ and obtain the *averaged beam displacement m_d*, from which the topological invariant can be inferred.[45,46] A topologically trivial lattice has an $m_d \sim 0$, as an indication of a zero Zak phase. A topological system will shift this value to $m_d \sim 0.5$, corresponding to a non-trivial π Zak phase.[45] Our collected results are shown in Fig. 2(c). We observe that for $\delta > 1$ ($d_1 < 30$ μm), the lattice is

topologically trivial, and the propagation shows a m_d around zero. For $\delta \sim 1$ ($d_1 \sim 30$ μm), a transition region without a well-defined topological phase is observed. For $\delta < 1.0$ ($d_1 > 30$ μm), the lattices express an averaged beam displacement around 0.5, implying a clear nontrivial Zak phase (see also the supplementary material). This is in very good agreement with the direct numerical simulations shown in Fig. 2(c) by an orange curve. Therefore, the wavelength-scan method gives us valuable information about the dynamics on a specific lattice and, in addition, it becomes a key and simple method to determine its topological phase experimentally.

The number of unit cells in the lattice affects the edge state properties: the fewer unit cells, the shorter the range of δ in which the edge states keep degenerate in β_z (see supplementary material). When the degeneracy is lifted, the two edge modes hybridize. Therefore, an input on one edge will coherently excite both modes and will result in periodic oscillations of the amplitude at the two edges on a very long dynamical scale. Then, an effective transfer of light from one edge to the other becomes possible.[23,24] To experimentally demonstrate this, we fabricate a topological lattice with 9 unit cells and distances $d_1 = 18$, $d_2 = 14$, and $d_v = 14$ μm ($t_1 = 0.30$ and $t_2 = 0.42$ cm^{-1} at 640 nm, and $\delta = 0.71$). The trivial lattice ($\delta = 1.40$) is obtained by inverting these distances to $d_1 = 14$ and $d_2 = 18$ μm. In this experiment, we decreased the distances to increase the coupling coefficients and favor faster transport in between the edges while staying in the non-degenerate situation. The inclusion of vertical next-nearest-neighbor (NNN) couplings would shift the energies for FB modes and, also, for the edge states, and the topological transfer would not be observable. The NNN hopping indeed does not destroy the edge states, but the definition of the winding number is not the same anymore[47] (see also supplementary material). Again, we use an SC laser source in the range of 610–740 nm and sweep the input wavelength in steps of 10 nm. We excite the system by injecting light at the B left edge waveguide, as shown in Fig. 3(a). For $\lambda \lesssim 670$ nm, the intensity profiles are well localized at the left edge, with most of the light intensity at the B sublattices, with a profile resembling the edge state [Fig. 1(e1)]. The edge state splitting manifests around $\lambda \approx 680$ nm, where we start observing a smooth population of the opposite edge with a very weak excitation of the lattice center (a weak background radiation is always observed due to the excitation of dispersive modes; see supplementary material). The connection in between both edge patterns [see Fig. 1(b) insets and (e)], with a B-site exponential decaying profile at the left surface and an A, C exponential profile at the right edge, becomes evident for ~710 nm. The spectral state transfer phenomenon starts occurring at $\lambda \gtrsim 720$ nm: the light injected at one edge is mostly transferred to the opposite edge. This shows a very interesting transport mechanism that does not require the light to explore the bulk modes of the lattice. In this case, the light transfers suddenly from one edge mode to the other without interacting with the lattice bulk modes. Due to the topological properties of this dimerized lattice, the edge-to-edge transfer dynamics are mainly governed by the topological edge states, with only a weak leak to dispersive modes.

To quantify the transfer, starting from a left edge B-site input excitation into the opposite right edge, we define the fidelity F for an edge-to-edge light transfer by measuring the normalized transferred intensity at the opposite lattice edge: $F \equiv (|A_{edge}|^2 + |C_{edge}|^2)/\sum_n P_n$. If all the light reaches the two rightmost sites, $F = 1$, and $F = 0$ in the fully opposite case. We show our results in Fig. 3(b), where we plot
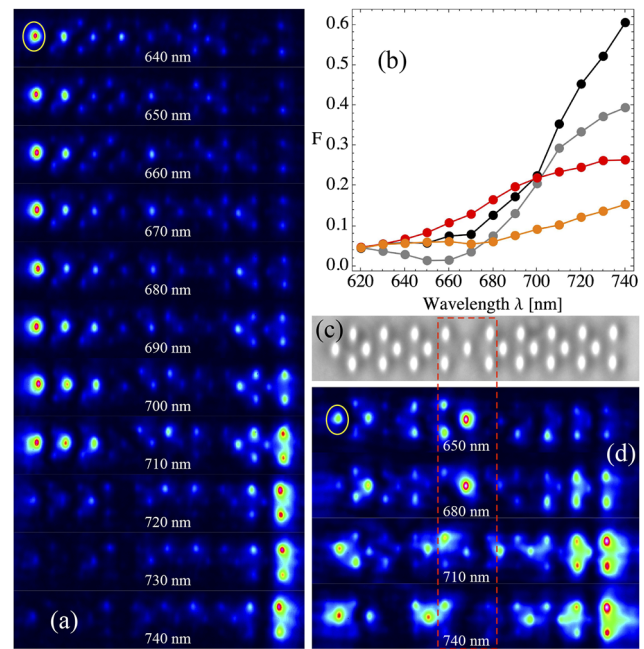
FIG. 3. (a) Output profiles of a non-trivial diamond photonic lattice at different λ's after a B-edge excitation (see yellow ellipse). (b) Fidelity vs wavelength for topological (black), trivial (gray), topological + defect (red), and trivial + defect (orange) lattices. (c) Microscope image of a topological lattice plus two coupling defects (see dashed rectangle). (d) Same as (a) for a topological lattice with a coupling defect.

the fidelity F vs λ for topological and trivial lattices. We observe how the topological (black) and trivial (gray) cases have a similar dynamical scale, i.e., both processes occur approximately at the same speed. However, the fidelity at the A, C surface is larger for the topological lattice (~61%). The trivial lattice presents a standard discrete diffraction pattern,[33] with the energy exploring the whole lattice while it moves from one edge into the other as the wavelength increases [similar to Fig. 2(a); see also the supplementary material]. Therefore, once the light arrives at the A, C right edge, it is reflected back due to the absence of the edge states. The fidelity in this case decreases to ~40%.

A remarkable feature of the state transfer between topological edge states is the resilience to disorder in the coupling constants. Although the fabrication process can produce random on-site or inter-site defects, we fabricate a couple of lattices with a symmetric coupling defect, as shown in Fig. 3(c). We design a different distance in between the fourth and fifth cells, and inside the fifth cell [see dashed rectangle in Fig. 3(c)]. Specifically, we set this distance to 23 μm, implying a coupling constant of 0.18 cm^{-1}. This corresponds to a strong impurity, considering the t_1 and t_2 values. Figure 3(d) shows a set of output images at the indicated values of λ for the topological lattice with a defect. We notice that this defect produces some reflection and trapping of energy at shorter wavelengths for 7 cm of propagation; consequently, not all the energy is edge-to-edge transferred. Despite this, a significant amount of light excites the topological right-edge state composed of A and C sites. The fidelity takes into account the effect of the defect on the transfer,

which is reduced to ~26% for the topological case, whereas it drops to ~15% for the trivial lattice (in this case, for $\lambda = 740$ nm).

These numbers show that a trivial lattice undergoes a stronger back reflection caused by the defect because the light explores the whole lattice and interacts strongly with it. On the other hand, in the topological case, the light does not need to interact with the bulk modes across the lattice, and it excites efficiently the edge state without the need to arrive at the boundary by standard transportation mechanisms. The fidelity is not perfect in any of the topological cases because a single *B*-site input always excites part of the dispersive spectrum, in which the modes extend over the entire lattice. Nonetheless, the important difference between the topological and trivial cases is the key to success for a topological state transfer process, which occurs due to the excitation of exponentially localized topological edge states, which exist at both edges simultaneously and deep into the gap of the lattice spectrum.

In comparison with the photonic realization of a Heisenberg spin chain of qubits, in which a state is transferred from one edge to the other with high fidelity,[48] our transfer protocol provides a more versatile tool when considering deliberate disorder in the coupling constants and a wide range of wavelengths for the incident beam. This could be a proof of concept for a long-distance photonic sensor that detects away from the interaction/excitation region and can be more robust against bulk imperfections.

IV. CONCLUSIONS

In this work, we used the wavelength-scan method as an important tool for investigating the dynamics of photonic waveguide lattices. We evidenced the nontrivial topology of dimerized diamond lattices by experimentally measuring the averaged beam displacement. In addition, we demonstrated an edge-to-edge transfer of light via a strong excitation of the lattice topological edge states. This transfer is based on an undriven protocol, in contrast with the one based on a driven 1D quasicrystal,[9] and is partially robust to defects across the lattice bulk. Furthermore, this lattice configuration could be used as a precise wavelength filter or as an efficient information transport mechanism. Considering very distant ports, a sequence of concatenated topological lattices could transform into a key solution for long-distance quantum communication protocols.[12,14] We became aware of a recent work reporting related transport properties in a SSH chain of split resonators.[49]

SUPPLEMENTARY MATERIAL

See supplementary material for both simulation at experimental details.

AUTHOR DECLARATIONS

Conflict of Interest

The authors have no conflicts to disclose.

Author Contributions

G.C.-A. and B.R. authors contributed equally to this work.

Gabriel Cáceres-Aravena: Conceptualization (equal); Data curation (equal); Formal analysis (equal); Investigation (equal); Visualization (equal). **Bastián Real**: Conceptualization (equal); Data curation (equal); Formal analysis (equal); Investigation (equal); Visualization (equal); Writing – original draft (equal); Writing – review & editing (equal). **Diego Guzmán-Silva**: Data curation (equal); Formal analysis (equal); Investigation (equal); Writing – original draft (equal). **Paloma Vildoso**: Investigation (equal). **Ignacio Salinas**: Investigation (equal). **Alberto Amo**: Formal analysis (equal); Funding acquisition (equal); Writing – original draft (equal). **Tomoki Ozawa**: Formal analysis (equal); Funding acquisition (equal); Writing – original draft (equal). **Rodrigo A. Vicencio**: Data curation (equal); Formal analysis (equal); Funding acquisition (equal); Investigation (equal); Methodology (equal); Resources (equal); Supervision (equal); Visualization (equal); Writing – original draft (equal); Writing – review & editing (equal).

DATA AVAILABILITY

The data that support the findings of this study are available from the corresponding author upon reasonable request.

REFERENCES

[1]B. Bahari, A. Ndao, F. Vallini, A. El Amili, Y. Fainman, and B. Kanté, "Nonreciprocal lasing in topological cavities of arbitrary geometries," Science **358**, 636–640 (2017).

[2]M. A. Bandres, S. Wittek, G. Harari, M. Parto, J. Ren, M. Segev, D. N. Christodoulides, and M. Khajavikhan, "Topological insulator laser: Experiments," Science **359**, aar4005 (2018).

[3]S. Barik, A. Karasahin, C. Flower, T. Cai, H. Miyake, W. DeGottardi, M. Hafezi, and E. Waks, "A topological quantum optics interface," Science **359**, 666–668 (2018).

[4]M. Jalali Mehrabad, A. P. Foster, R. Dost, E. Clarke, P. K. Patil, A. M. Fox, M. S. Skolnick, and L. R. Wilson, "Chiral topological photonics with an embedded quantum emitter," Optica **7**, 1690 (2020).

[5]S. Mittal, E. A. Goldschmidt, and M. Hafezi, "A topological source of quantum light," Nature **561**, 502–506 (2018).

[6]S. Mittal, G. Moille, K. Srinivasan, Y. K. Chembo, and M. Hafezi, "Topological frequency combs and nested temporal solitons," Nat. Phys. **17**, 1169–1176 (2021).

[7]A. Blanco-Redondo, B. Bell, D. Oren, B. J. Eggleton, and M. Segev, "Topological protection of biphoton states," Science **362**, 568–571 (2018).

[8]J.-L. Tambasco, G. Corrielli, R. J. Chapman, A. Crespi, O. Zilberberg, R. Osellame, and A. Peruzzo, "Quantum interference of topological states of light," Sci. Adv. **4**, eaat3187 (2018).

[9]Y. E. Kraus, Y. Lahini, Z. Ringel, M. Verbin, and O. Zilberberg, "Topological states and adiabatic pumping in quasicrystals," Phys. Rev. Lett. **109**, 106402 (2012).

13 August 2023 13:13:42

[10]W. Liu, C. Wu, Y. Jia, S. Jia, G. Chen, and F. Chen, "Observation of edge-to-edge topological transport in a photonic lattice," Phys. Rev. A **105**, L061502 (2022).

[11]R. J. Chapman, M. Santandrea, Z. Huang, G. Corrielli, A. Crespi, M.-H. Yung, R. Osellame, and A. Peruzzo, "Experimental perfect state transfer of an entangled photonic qubit," Nat. Commun. **7**, 11339 (2016).

[12]N. Lang and H. P. Büchler, "Topological networks for quantum communication between distant qubits," npj Quantum Inf. **3**, 47 (2017).

[13]X. Li, Y. Ma, J. Han, T. Chen, Y. Xu, W. Cai, H. Wang, Y. P. Song, Z.-Y. Xue, Z.-q. Yin, and L. Sun, "Perfect quantum state transfer in a superconducting qubit chain with parametrically tunable couplings," Phys. Rev. Appl. **10**, 054009 (2018).

[14]F. Mei, G. Chen, L. Tian, S.-L. Zhu, and S. Jia, "Robust quantum state transfer via topological edge states in superconducting qubit chains," Phys. Rev. A **98**, 012331 (2018).

[15]L. Qi, G.-L. Wang, S. Liu, S. Zhang, and H.-F. Wang, "Engineering the topological state transfer and topological beam splitter in an even-sized Su-Schrieffer-Heeger chain," Phys. Rev. A **102**, 022404 (2020).

[16]Z.-G. Chen, W. Tang, R.-Y. Zhang, Z. Chen, and G. Ma, "Landau-Zener transition in the dynamic transfer of acoustic topological states," Phys. Rev. Lett. **126**, 054301 (2021).

[17]N. E. Palaiodimopoulos, I. Brouzos, F. K. Diakonos, and G. Theocharis, "Fast and robust quantum state transfer via a topological chain," Phys. Rev. A **103**, 052409 (2021).

[18]P. Boross, J. K. Asbóth, G. Széchenyi, L. Oroszlány, and A. Pályi, "Poor man's topological quantum gate based on the Su-Schrieffer-Heeger model," Phys. Rev. B **100**, 045414 (2019).

[19]S. Longhi, "Topological pumping of edge states via adiabatic passage," Phys. Rev. B **99**, 155150 (2019).

[20]F. M. D'Angelis, F. A. Pinheiro, D. Guéry-Odelin, S. Longhi, and F. Impens, "Fast and robust quantum state transfer in a topological Su-Schrieffer-Heeger chain with next-to-nearest-neighbor interactions," Phys. Rev. Res. **2**, 033475 (2020).

[21]M. P. Estarellas, I. D'Amico, and T. P. Spiller, "Topologically protected localised states in spin chains," Sci. Rep. **7**, 42904 (2017).

[22]J. Yuan, C. Xu, H. Cai, and D.-W. Wang, "Gap-protected transfer of topological defect states in photonic lattices," APL Photonics **6**, 030803 (2021).

[23]N. K. Efremidis, "Topological photonic Su-Schrieffer-Heeger-type coupler," Phys. Rev. A **104**, 053531 (2021).

[24]S. de Léséleuc, V. Lienhard, P. Scholl, D. Barredo, S. Weber, N. Lang, H. P. Büchler, T. Lahaye, and A. Browaeys, "Observation of a symmetry-protected topological phase of interacting bosons with Rydberg atoms," Science **365**, 775–780 (2019).

[25]A. A. Arkhipova, S. K. Ivanov, S. A. Zhuravitskii, N. N. Skryabin, I. V. Dyakonov, A. A. Kalinkin, S. P. Kulik, V. O. Kompanets, S. V. Chekalin, Y. V. Kartashov, and V. N. Zadkov, "Observation of nonlinearity-controlled switching of topological edge states," Nanophotonics **11**, 3653–3661 (2022).

[26]J. Zurita, C. E. Creffield, and G. Platero, "Fast quantum transfer mediated by topological domain walls," Quantum **7**, 1043 (2023).

[27]J. Vidal, B. Douçot, R. Mosseri, and P. Butaud, "Interaction induced delocalization for two particles in a periodic potential," Phys. Rev. Lett. **85**, 3906–3909 (2000).

[28]C. E. Creffield and G. Platero, "Coherent control of interacting particles using dynamical and Aharonov–Bohm phases," Phys. Rev. Lett. **105**, 086804 (2010).

[29]G. Cáceres-Aravena, D. Guzmán-Silva, I. Salinas, and R. A. Vicencio, "Controlled transport based on multiorbital Aharonov–Bohm photonic caging," Phys. Rev. Lett. **128**, 256602 (2022).

[30]A. Szameit, D. Blömer, J. Burghoff, T. Schreiber, T. Pertsch, S. Nolte, A. Tünnermann, and F. Lederer, "Discrete nonlinear localization in femtosecond laser written waveguides in fused silica," Opt. Express **13**, 10552–10557 (2005).

[31]S. Mukherjee and R. R. Thomson, "Observation of robust flat-band localization in driven photonic rhombic lattices," Opt. Lett. **42**, 2243–2246 (2017).

[32]L. Tang, D. Song, S. Xia, S. Xia, J. Ma, W. Yan, Y. Hu, J. Xu, D. Leykam, and Z. Chen, "Photonic flat-band lattices and unconventional light localization," Nanophotonics **9**, 1161–1176 (2020).

[33]R. A. V. Poblete, "Photonic flat band dynamics," Adv. Phys.: X **6**, 1878057 (2021).

[34]G. Cáceres-Aravena, B. Real, D. Guzmán-Silva, A. Amo, L. E. F. Foa Torres, and R. A. Vicencio, "Experimental observation of edge states in SSH-stub photonic lattices," Phys. Rev. Res. **4**, 013185 (2022).

[35]W. P. Su, J. R. Schrieffer, and A. J. Heeger, "Solitons in polyacetylene," Phys. Rev. Lett. **42**, 1698–1701 (1979).

[36]D. Bercioux, O. Dutta, and E. Rico, "Solitons in one-dimensional lattices with a flat band," Ann. Phys. **529**, 1600262 (2017).

[37]A. Ramachandran, A. Andreanov, and S. Flach, "Chiral flat bands: Existence, engineering, and stability," Phys. Rev. B **96**, 161104(R) (2017).

[38]K. M. Davis, K. Miura, N. Sugimoto, and K. Hirao, "Writing waveguides in glass with a femtosecond laser," Opt. Lett. **21**, 1729–1731 (1996).

[39]N. Malkova, I. Hromada, X. Wang, G. Bryant, and Z. Chen, "Observation of optical Shockley-like surface states in photonic superlattices," Opt. Lett. **34**, 1633–1635 (2009).

[40]L.-C. Wang, Y. Chen, M. Gong, F. Yu, Q.-D. Chen, Z.-N. Tian, X.-F. Ren, and H.-B. Sun, "Edge state, localization length, and critical exponent from survival probability in topological waveguides," Phys. Rev. Lett. **129**, 173601 (2022).

[41]A. A. Sukhorukov, D. N. Neshev, and Y. S. Kivshar, "Shaping and control of polychromatic light in nonlinear photonic lattices," Opt. Express **15**, 13058–13076 (2007).

[42]F. Dreisow, M. Heinrich, A. Szameit, S. Doering, S. Nolte, A. Tuennermann, S. Fahr, and F. Lederer, "Spectral resolved dynamic localization in curved fs laser written waveguide arrays," Opt. Express **16**, 3474 (2008).

[43]A. Szameit, I. L. Garanovich, M. Heinrich, A. A. Sukhorukov, F. Dreisow, T. Pertsch, S. Nolte, A. Tünnermann, and Y. S. Kivshar, "Polychromatic dynamic localization in curved photonic lattices," Nat. Phys. **5**, 271–275 (2009).

[44]U. Naether, S. Stützer, R. A. Vicencio, M. I. Molina, A. Tünnermann, S. Nolte, T. Kottos, D. N. Christodoulides, and A. Szameit, "Experimental observation of superdiffusive transport in random dimer lattices," New J. Phys. **15**, 013045 (2013).

[45]S. Longhi, "Probing one-dimensional topological phases in waveguide lattices with broken chiral symmetry," Opt. Lett. **43**, 4639 (2018).

[46]Z.-Q. Jiao, S. Longhi, X.-W. Wang, J. Gao, W.-H. Zhou, Y. Wang, Y.-X. Fu, L. Wang, R.-J. Ren, L.-F. Qiao, and X.-M. Jin, "Experimentally detecting quantized Zak phases without chiral symmetry in photonic lattices," Phys. Rev. Lett. **127**, 147401 (2021).

[47]R. S. K. Mong and V. Shivamoggi, "Edge states and the bulk-boundary correspondence in Dirac Hamiltonians," Phys. Rev. B **83**, 125109 (2011).

[48]A. Perez-Leija, R. Keil, A. Kay, H. Moya-Cessa, S. Nolte, L.-C. Kwek, B. M. Rodríguez-Lara, A. Szameit, and D. N. Christodoulides, "Coherent quantum transport in photonic lattices," Phys. Rev. A **87**, 012309 (2013).

[49]Y.-H. Chang, N. D. Rivera Torres, S. Figueroa Manrique, R. A. Robles Robles, V. C. Silalahi, C.-S. Wu, G. Wang, G. Marcucci, L. Pilozzi, C. Conti, R.-K. Lee, and W. Kuo, arXiv:2004.09282 [cond-mat.mes-hall].